Improved method of calculating *ab initio* high-temperature thermodynamic properties with application to ZrC

Andrew Ian Duff* and Theresa Davey
Department of Materials, Thomas Young Centre, Imperial College London, Exhibition Road, London SW7 2AZ, UK

Dominique Korbmacher, Albert Glensk, Blazej Grabowski, and Jörg Neugebauer
Max-Planck-Institut für Eisenforschung, Max-Planck-Strasse 1, Düsseldorf 40237, Germany

Michael W. Finnis
Department of Materials and Department of Physics, Thomas Young Centre, Imperial College London, Exhibition Road, London SW7 2AZ, UK

(Received 15 May 2015; published 30 June 2015)

Thermodynamic properties of ZrC are calculated up to the melting point ($T^{\mathrm{melt}} \approx 3700$ K), using density functional theory (DFT) to obtain the fully anharmonic vibrational contribution, and including electronic excitations. A significant improvement is found in comparison to results calculated within the quasiharmonic approximation. The calculated thermal expansion is in better agreement with experiment and the heat capacity reproduces rather closely a CALPHAD estimate. The calculations are presented as an application of a development of the *upsampled thermodynamic integration using Langevin dynamics* (UP-TILD) approach. This development, referred to here as *two-stage upsampled thermodynamic integration using Langevin dynamics* (TU-TILD), is the inclusion of tailored interatomic potentials to characterize an intermediate reference state of anharmonic vibrations on a two-stage path of thermodynamic integration between the original DFT quasiharmonic free energy and the fully anharmonic DFT free energy. This approach greatly accelerates the convergence of the calculation, giving a factor of improvement in efficiency of ∼50 in the present case compared to the original UP-TILD approach, and it can be applied to a wide range of materials.

DOI: 10.1103/PhysRevB.91.214311 PACS number(s): 63.20.Ry, 65.40.Ba, 81.05.Je

I. INTRODUCTION

Zirconium carbide (ZrC) belongs to the class of ultrahigh-temperature ceramics (UHTCs), which have a desirable combination of metallic and ceramic properties, namely high thermal and electrical conductivities, high toughness, and good corrosion/oxidation resistance [1]. Given this combination of properties, applications in extreme environments, such as those encountered by materials within nuclear reactors and on shuttle reentry and ultrasonic vehicles, are being actively investigated.

Despite their wide use, however, the thermodynamic properties and phase stabilities of UHTCs are poorly characterized, due to the large experimental errors associated with measuring the onset of melting at such high temperatures. This also affects the phase characterization of ternary compounds such as the $M_{n+1}AX_n$ (MAX) phases [2], since many binary UHTCs constitute the end members of the ternary systems containing these MAX phases.

In order to learn more about the phase stabilities of UHTCs it would be desirable to perform *ab initio* calculations of their thermodynamic properties up to the melting point. Such results, along with the available experimental data, could then be used in subsequent work to perform CALPHAD reassessments of UHTC phase diagrams. However, accurate finite-temperature *ab initio* calculations on UHTCs pose a significant challenge due to the strongly anharmonic lattice vibrations expected for such materials. The standard approach to calculating the vibrational contribution to free energy with density functional theory (DFT) is the so-called *quasiharmonic approximation*. This is a harmonic model of the normal modes of the crystal, in which the harmonic frequencies are renormalized simply by calculating them at fixed volumes covering the range of thermal expansion. At any given volume these frequencies enter the standard model for the harmonic free energy as a function of temperature and, together with the contribution due to electronic excitations, this free energy can be minimized as a function of volume for any desired temperature, yielding a prediction of the free energy versus temperature from which all other thermophysical properties can be derived. However, it has long been realized that at temperatures higher than about half the melting point, a truly anharmonic contribution should be included. This was first attempted with DFT calculations in the SCAILD method (self-consistent *ab initio* lattice dynamics) [3]. However, the accuracy of the approximation of renormalized harmonic frequencies in this approach is hard to evaluate [4]. A fully anharmonic correction with DFT and classical lattice dynamics was introduced by Grabowski and coworkers [5]. This is the *upsampled thermodynamic integration using Langevin dynamics* (UP-TILD) approach, on which the research reported here is based. Another promising recent approach by Montserrat *et al.* [6] uses a quantum mechanical perturbation theory to include the effect of phonon-phonon interactions to second order beyond a mean-field theory. This has the advantage of including the quantum dynamics of the vibrations also in the anharmonic contribution, and the associated ability to evaluate expectation values of many quantum mechanical

*andrew.duff@imperial.ac.uk

operators, whereas we can only include quantized vibrations at the harmonic level. However, whereas our anharmonic correction is based on purely classical dynamics, it is nonperturbative, and with the enhancement of the UP-TILD method to be described here, its computational requirements are modest.

Our chosen approach, which operates within the framework of DFT, makes the calculation of *ab initio* fully anharmonic properties tractable by (i) using thermodynamic integration (TI) to calculate the anharmonic free energy employing DFT quasiharmonic calculations as a reference, and (ii) applying upsampling techniques to enable more efficient calculation of DFT energies. Even within this computationally more amenable framework, however, the calculation of thermal properties for UHTCs still remains a significant challenge due to the strong anharmonicity present in these materials.

To address this challenge, a further development is presented in the present article in which the TI is performed in two stages, starting from the quasiharmonic reference state. The first stage switches the system into one executing anharmonic vibrations described by an empirical interatomic potential. In a second stage the empirical interatomic potential is switched to the DFT energy in a constant-temperature molecular dynamics (MD) simulation (similar to the approach used by Alfè *et al.* in calculating the melting curve of iron [7]). By fitting the potential directly to the full DFT internal energy during a Langevin molecular dynamics (LD) run, a better anharmonic starting point for the second stage of the TI is provided, and a sizable gain in efficiency is achieved compared to the original UP-TILD formulation. The second stage of the TI is far more expensive computationally than the first, since for the first stage of TI a number of static DFT calculations are done beforehand, for the purpose of obtaining the quasiharmonic dynamical matrix, and no further DFT calculations are required during this stage. Only during the second stage are time-consuming DFT MD runs required, but now the phase space sampled by the classical potentials is closer to the DFT sampling, and the convergence of the TI is much faster. This efficiency gain makes the *ab initio*, fully anharmonic calculations of the thermal properties of ZrC ($T^{\mathrm{melt}} \approx 3700$ K) [8] feasible, and will enable similar calculations for other UHTC compounds to be performed with a modest computer budget. It is worth emphasizing at this point that the particular interatomic potentials used in these calculations may affect the rate of convergence but will have no effect on the converged results, because they are used purely to provide intermediate reference states from which to reach the final results more efficiently. We have tested both embedded atom method (EAM) and modified embedded atom method (MEAM) potentials.

The structure of the paper is as follows: In Sec. II the theoretical background to the work is presented, including a discussion of both the original UP-TILD formulation and a description of our approach. In Sec. III, the interatomic potential formalism and a sample parametrization is presented. The fully anharmonic thermal properties for ZrC are reported in Sec. IV, along with a discussion of the improvement in efficiency provided by our approach. Concluding remarks are given in Sec. V.

II. THEORETICAL BACKGROUND

A. The free energy

The starting point for determining thermal properties at finite temperature is the Helmholtz free energy $F(V,T)$, where V and T represent volume and temperature, respectively. Once this has been calculated for the relevant range of V and T, the thermal expansion $V_{\mathrm{eq}}(T)$ and the heat capacity $C_P(T)$ can be derived using

$$\left.\frac{\partial F(V,T)}{\partial V}\right|_{V_{\mathrm{eq}}(T)} = 0, \quad C_P(T) = -T \left.\frac{\partial^2 F(V,T)}{\partial T^2}\right|_{V_{\mathrm{eq}}(T)}. \tag{1}$$

In the present work, $F(V,T)$ is calculated from first principles, within the framework of density functional theory (DFT). To perform the calculations, it is necessary to express the total free energy as the following separate parts:

$$F(V,T) = E^{\mathrm{tot}}(V) + F^{\mathrm{el}}(V,T) + F^{\mathrm{qh}}(V,T) + F^{\mathrm{ah}}(V,T), \tag{2}$$

where $E^{\mathrm{tot}}(V)$ is the total energy at $T = 0$ K, $F^{\mathrm{el}}(V,T)$ is the finite-temperature electronic free energy, $F^{\mathrm{qh}}(V,T)$ is the free energy due to atomic vibrations, computed within the quasiharmonic approximation, and $F^{\mathrm{ah}}(V,T)$ is the anharmonic free energy, which combined with the quasiharmonic free energy provides the full vibrational free energy: $F^{\mathrm{vib}}(V,T) = F^{\mathrm{qh}}(V,T) + F^{\mathrm{ah}}(V,T)$. The first three contributions can be calculated straightforwardly [9–11] and do not represent a challenge computationally. In particular, the basis for obtaining the electronic contribution is the finite-temperature extension of DFT by Mermin [12] which provides a mapping of the interacting electronic thermodynamic ground state at a certain temperature to the electronic density. In combination with the Kohn-Sham approach [13], finite-temperature DFT allows the calculation of the electronic entropy within an effective single-electron approach limited only by the accuracy of the exchange-correlation functional. Specifically, the finite-temperature charge density is obtained as $\rho(\vec{r},T) = \sum_i f_i(T)|\psi_i(\vec{r})|^2$ with $f_i(T)$ the Fermi-Dirac occupation numbers and ψ_i the one-particle Kohn-Sham eigenfunctions obtained using the above charge density and the appropriate exchange-correlation functional. Thus, the electronic density of states is not a ground state property but becomes temperature dependent.

Calculating the anharmonic free energy, and thus the full vibrational free energy, represents a considerable challenge, however, and is addressed in the present work within a reformulated version of the UP-TILD approach. A brief summary of the original UP-TILD approach is presented in the following section, followed by a description of our approach.

B. UP-TILD approach

Within the original UP-TILD formulation [5], thermodynamic integration (TI) is used to calculate the anharmonic free energy for a particular V and T using the quasiharmonic free

energy as a reference state:

$$F^{\mathrm{ah}} = \int_0^1 d\lambda \left[\left\langle E_{\mathrm{low}}^{\mathrm{DFT}} - E^{\mathrm{qh}} \right\rangle_\lambda + \langle \Delta E \rangle_\lambda^{\mathrm{UP}} \right], \tag{3}$$

where $E_{\mathrm{low}}^{\mathrm{DFT}}$ and E^{qh} are full DFT and DFT quasiharmonic energies, respectively, the latter being generated from the dynamical matrix, as required for every configuration of the atoms during the LD run. The angular braces denote a canonical ensemble average taken over a set of atomic configurations generated from LD runs, using either quasiharmonic atomic forces ($\lambda = 0$), full DFT atomic forces ($\lambda = 1$), or a linear combination of the two ($0 < \lambda < 1$). The DFT calculations used to compute $\langle E_{\mathrm{low}}^{\mathrm{DFT}} - E^{\mathrm{qh}} \rangle_\lambda$ use "reduced" DFT parameters (energy cutoff and k-points sampling) which, while sufficiently well converged to provide accurate atomic forces, result in energies which have an almost configuration-independent offset with respect to the fully converged energies. This offset is corrected for by the second term,

$$\langle \Delta E \rangle_\lambda^{\mathrm{UP}} = \frac{1}{N} \sum_i^N \left(E_{\mathrm{high}}^{\mathrm{DFT}} - E_{\mathrm{low}}^{\mathrm{DFT}} \right), \tag{4}$$

where $E_{\mathrm{high}}^{\mathrm{DFT}}$ is the DFT energy evaluated using fully converged DFT parameters, and where only a small number of configurations ($N \approx 5$) are required to evaluate this term. In the above, all the energies $E_{\mathrm{low}}^{\mathrm{DFT}}$, $E_{\mathrm{high}}^{\mathrm{DFT}}$, and E^{qh} are referenced with respect to their corresponding values at $T = 0$ K.

The use of reduced parameters in calculating $\langle E_{\mathrm{low}}^{\mathrm{DFT}} - E^{\mathrm{qh}} \rangle_\lambda$, combined with the use of TI, provides a scheme for calculating the anharmonic free energy which is four orders of magnitude more efficient than a direct, MD evaluation of the full vibrational free energy [5].

C. TU-TILD approach

The *two-stage upsampled thermodynamic integration using Langevin dynamics* (TU-TILD) approach described here employs interatomic potentials to create an intermediate reference state, making an efficient bridge from the quasiharmonic reference state to the full anharmonic vibrational free energy of Eq. (3). These classical potentials are generated by fitting to the DFT energies $E_{\mathrm{low}}^{\mathrm{DFT}}$ of a DFT-LD run for a particular V and T. The full anharmonic contribution to the free energy is then calculated in the following two stages:

$$\begin{aligned} F^{\mathrm{ah}} = & \int_0^1 d\lambda_1 [\langle E^{\mathrm{pot}} - E^{\mathrm{qh}} \rangle_{\lambda_1}] \\ & + \int_0^1 d\lambda_2 \left[\left\langle E_{\mathrm{low}}^{\mathrm{DFT}} - E^{\mathrm{pot}} \right\rangle_{\lambda_2} + \langle \Delta E \rangle_{\lambda_2}^{\mathrm{UP}} \right], \end{aligned} \tag{5}$$

where the first term now provides the difference between the free energies described by the DFT quasiharmonic dynamical matrix and by the classical potential. Here, E^{pot} is the energy calculated using the potential, which as with the other energies is referenced with respect to the $T = 0$ K energy. For the first term, the forces used to generate the atomic configurations vary linearly as a function of λ_1 from quasiharmonic forces ($\lambda_1 = 0$) to potential forces ($\lambda_1 = 1$). Since this term does not involve any explicit DFT calculations it can be calculated with minimal computational expense. For the second ensemble average $\langle E_{\mathrm{low}}^{\mathrm{DFT}} - E^{\mathrm{pot}} \rangle_{\lambda_2}$ the forces vary linearly from potential forces ($\lambda_2 = 0$) to full DFT forces ($\lambda_2 = 1$).

Since the number of terms required to evaluate $\langle E_{\mathrm{low}}^{\mathrm{DFT}} - E^{\mathrm{pot}} \rangle_{\lambda_2}$ to a given precision is proportional to the variance $\sigma(E_{\mathrm{low}}^{\mathrm{DFT}} - E^{\mathrm{pot}})^2$, deriving a potential which minimizes this variance should allow for the calculation of $\langle E_{\mathrm{low}}^{\mathrm{DFT}} - E^{\mathrm{pot}} \rangle_{\lambda_2}$ using significantly fewer configurations, providing a more efficient scheme for the calculation of the anharmonic free energy.

III. INTERATOMIC POTENTIALS

A. Modified embedded atom method

The potentials optimized within this work have been derived within the modified embedded atom method (MEAM) formalism [14–16], which is based on the embedded atom method (EAM) [17] but with the additional inclusion of angular forces. MEAM potentials have been derived and applied to various elements and alloys encompassing a wide range of bonding characteristics [18,19]. In the present work, the reference-free formulation of the MEAM [20] is used as it removes the need to specify a reference structure, which otherwise restricts the form that the pair potentials can take. This enables greater variational freedom in the fitting of energies and atomic forces.

Within the reference-free MEAM formalism, the total energy of a system of N atoms is expressed as

$$E = \sum_{i=1}^N E_{\alpha_i}^{\mathrm{emb}}(\rho_i) + \frac{1}{2} \sum_{i \neq j}^N \phi_{\alpha_i,\alpha_j}(r_{ij}), \tag{6}$$

$$E_\alpha^{\mathrm{emb}}(\rho) = a_\alpha \rho^{\frac{1}{2}} + b_\alpha \rho^2 + c_\alpha \rho^3, \tag{7}$$

$$\rho_i = \frac{2\rho_i^{(0)}}{1 + e^{-\tau_i}}, \tag{8}$$

$$\tau_i = \sum_{l=1}^3 t_i^{(l)} \left(\frac{\rho_i^{(l)}}{\rho_i^{(0)}} \right)^2, \tag{9}$$

where $\phi_{\alpha_i,\alpha_j}(r_{ij})$ is the pair potential between atoms i and j with separation r_{ij}, $E_\alpha^{\mathrm{emb}}(\rho_i)$ is the embedding energy function, ρ_i is the background density at site i, $\rho_i^{(0)}$ is the sum over partial densities as encountered in typical EAM potentials,

$$\rho_i^{(0)} = \sum_{j \neq i}^N f_{\alpha_j}^{(0)}(r_{ij}), \tag{10}$$

and where $\rho_i^{(l>0)}$ are angular contributions to the background density specific to the MEAM approach (setting these to zero recovers the standard EAM formalism). The latter introduces bond angles (θ_{jik}) into the formalism:

$$\left(\rho_i^{(l)}\right)^2 = \sum_{j,k(\neq i)}^N f_{\alpha_j}^{(l)}(r_{ij}) f_{\alpha_k}^{(l)}(r_{ik}) P^{(l)}(\cos\theta_{jik}), \tag{11}$$

where $f_{\alpha_i}^{(l>0)}$ are termed the *partial* background density contributions and $P^{(l)}$ ($l = 0, \ldots, 3$) are Legendre polynomials: $P^{(0)}(x) = 1$, $P^{(1)}(x) = x$, $P^{(2)}(x) = (3x^2 - 1)/2$, and

$P^{(3)}(x) = (5x^5 - 3x)/2$. Although these functions are conventionally referred to as "electron" densities, we do not suppose they have any relation to the real electron density, and regard them purely as empirical fitting functions. The partial density contributions and also the pair potentials are parametrized as sums over cubic terms:

$$f_{\alpha_i}^{(l)}(r) = \sum_{n=1}^{2} a_{\alpha_i}^{(n,l)} \left(r_{\alpha_i}^{(n,l)} - r\right)^3 \Theta\left(r_{\alpha_i}^{(n,l)} - r\right), \quad (12)$$

$$\phi_{\alpha_i,\alpha_j}^{(l)}(r) = \sum_{n=1}^{2} b_{\alpha_i,\alpha_j}^{(n)} \left(s_{\alpha_i,\alpha_j}^{(n)} - r\right)^3 \Theta\left(s_{\alpha_i,\alpha_j}^{(n)} - r\right), \quad (13)$$

where $a_{\alpha_i}^{(n,l)}$, $b_{\alpha_i,\alpha_j}^{(n)}$, $r_{\alpha_i}^{(n,l)}$, and $s_{\alpha_i,\alpha_j}^{(n)}$ are parameters to be optimized and where $\Theta(r' - r)$ is a step function, providing a cutoff for $r' > r$.

Note that in the present work, two pairwise terms are used for each of the partial density contributions and pair potentials. In addition, a maximum cutoff radius is imposed: $r_{\alpha_i}^{(n,l)}, s_{\alpha_i,\alpha_j}^{(n)} < 4.4$ Å, so that up to second-nearest-neighbor interactions are included in the potential (as well as a small fraction of third-nearest-neighbor interactions due to thermal fluctuations) [21].

B. Fitting strategy

Rather than generating potentials for all V and T across which the anharmonic free energy is to be calculated, potentials are instead optimized only at $T = 3800$ K (the largest temperature to be considered in the subsequent anharmonic calculations). For each value of V, the $T = 3800$ K potential is then used to provide the intermediate reference state not just at the melting point but also for all other values of T. This strategy reduces the overall computational cost of generating the potentials, which must be balanced against the marginal improvement in efficiency in using temperature-dependent potentials for the calculation of the anharmonic free energy.

The MEAM potentials were optimized using the MEAMfit fitting code [22], with the variance in the error of the fitted energies taken as the objective function to be minimized:

$$\sigma\left(E_{\text{low}}^{\text{DFT}} - E^{\text{pot}}\right)^2 = \left\langle \left(E_{\text{low}}^{\text{DFT}} - E^{\text{pot}}\right)^2 \right\rangle - \left\langle E_{\text{low}}^{\text{DFT}} - E^{\text{pot}} \right\rangle^2, \quad (14)$$

where the ensemble averages are taken over fitting sets each containing 1000 $E_{\text{low}}^{\text{DFT}}$ energies. These energies and their associated atomic configurations are generated from DFT LD runs, and can be reused when the $\lambda = 1$ ensemble averages of Eq. (5) are calculated in Sec. IV. Typical optimized values of $\sigma(E_{\text{low}}^{\text{DFT}} - E^{\text{pot}})$ are found to be of the order ∼4 meV/atom at $T = 3800$ K. As a specific example, the optimized potential for $V = 14.26$ Å^3/atom and $T = 3800$ K is presented in Table I , for which a value $\sigma(E_{\text{low}}^{\text{DFT}} - E^{\text{pot}}) = 3.4$ meV/atom was obtained.

TABLE I. Parametrization of the ZrC MEAM potential used for $V = 14.26$ Å^3/atom and $T = 3800$ K (see main text for function definitions and descriptions).

	Embedding functions		
	a (eV)	b (eV)	c (eV)
$E_{\text{Zr}}^{\text{emb}}$	0.1746	-2.2773×10^{-5}	-1.7412×10^{-6}
$E_{\text{C}}^{\text{emb}}$	2.3486	-4.8510×10^{-4}	1.7512×10^{-9}

	Pairwise functions			
	$a^{(1)}$	$b^{(1)}$ (Å)	$a^{(2)}$	$b^{(2)}$ (Å)
$f_{\text{Zr}}^{(l=0)}$	−49.5413	2.0981	5.0457	3.5321
$f_{\text{Zr}}^{(l=1)}$	−7.3363	3.3746	7.1910	3.5267
$f_{\text{Zr}}^{(l=2)}$	1.8025	3.3967	18.0434	2.4384
$f_{\text{Zr}}^{(l=3)}$	−6.2369	3.4621	5.0754	3.9220
$f_{\text{C}}^{(l=0)}$	−13.3902	2.6382	0.5372	4.4000
$f_{\text{C}}^{(l=1)}$	−2.0187	3.8652	−0.8673	2.6386
$f_{\text{C}}^{(l=2)}$	−9.5178	4.2405	7.5633	4.3771
$f_{\text{C}}^{(l=3)}$	−5.8925	3.7789	3.7078	3.6166
	$a^{(1)}$ (eV)	$b^{(1)}$ (Å)	$a^{(2)}$ (eV)	$b^{(2)}$ (Å)
$\phi_{\text{Zr,Zr}}$	1.2909	3.7638	3.9528	2.1817
$\phi_{\text{Zr,C}}$	3.8086	2.4008	1.6265	3.1136
$\phi_{\text{C,C}}$	20.1904	4.3969	− 19.6642	4.4000

	Background density prefactors	
	Zr	C
$t_\alpha^{(1)}$	5.7609	4.1455
$t_\alpha^{(2)}$	−10.7622	−1.0892
$t_\alpha^{(3)}$	−0.7883	−0.4435

IV. CALCULATIONS

A. Computational details

The DFT calculations were performed with the VASP software package [23–26] using both LDA and GGA exchange-correlation functionals. The projector-augmented wave method is used [27,28], with 4*s*- and 4*p*-Zr electrons included as valence states. ZrC has a simple cubic (rocksalt) structure, and in the present case is taken to have a stoichiometric composition (although experimentally it is normally found to have a slightly substoichiometric composition, ZrC_x, with $x = 0.95$–1). The plane-wave cutoff and the k-point convergence were adjusted separately for each of the free energy contributions to ensure convergence of the free energy contributions to within ±1 meV/atom at the melting point in each case. The converged values of the DFT parameters along with the supercell dimensions for each free energy contribution are reported in Table II.

The quasiharmonic contribution, $F^{\text{qh}}(V,T)$, is calculated using the direct method [29], with a mesh consisting of five volumes ($V = 12.85$ Å^3/atom, 13.23 Å^3/atom, 13.47 Å^3/atom, 13.83 Å^3/atom, and 13.87 Å^3/atom for the GGA).

For $F^{\text{el}}(V,T)$, Mermin's finite-temperature formulation of DFT is used, with a mesh of 10 volumes and 10 temperatures constructed in the relevant region. Temperatures were chosen to span the range (0 K, ..., 3800 K). Note that for these calculations as well as others, a slightly larger upper temperature limit of 3800 K is used ($T^{\text{melt}} \approx 3700$ K) to provide a better basis for fitting analytic functions to the free energy contribu-

TABLE II. The k-point Monkhorst-Pack meshes and plane-wave cutoffs used to calculate $E^{\rm tot}(V)$, $F^{\rm el}(V,T)$, $F^{\rm qh}(V,T)$, and $F^{\rm ah}(V,T)$, as defined in Eq. (2). Supercell sizes in units of the 8-atom conventional cubic cell are also shown.

	Supercell size	k-point grid	$E^{\rm cut}$ (eV)
$E^{\rm tot}(V)$	$1\times1\times1$	$16\times16\times16$	700
$F^{\rm el}(V,T)$	$1\times1\times1$	$24\times24\times24$	700
$F^{\rm qh}(V,T)$	$2\times2\times2$	$8\times8\times8$	700
$F^{\rm ah}(V,T)$	$2\times2\times2$	$8\times8\times8$	700

tions. The temperature range in turn determines the relevant range for the volumes: $V_{\rm eq}(T=0\ {\rm K}),\ldots,V_{\rm eq}(T=3800\ {\rm K})$, with $V_{\rm eq}(T=3800\ {\rm K})\approx1.15V_{\rm eq}(T=0\ {\rm K})$. A fourth-order polynomial in terms of V and T was then used to fit $F^{\rm el}(V,T)$ ($\sum_{i,j}V^iT^j$ with $i\geqslant0$, $j\geqslant1$, and $i+j\leqslant4$).

For the fully anharmonic calculations, the same set of V values as for the quasiharmonic calculations are used, and five values are used to span the temperature range ($T=760$ K, 1900 K, 2500 K, 3200 K, and 3800 K). Furthermore, to perform the numerical integration over the coupling parameter λ_2 [second term in Eq. (5)], five values are used: $\lambda_2=0$, 0.15, 0.5, 0.85, and 1. These values were chosen to reflect the dependence of $\langle E^{\rm DFT}_{\rm low}-E^{\rm pot}\rangle_\lambda$ on λ, which mainly followed a linear dependence except for slight deviations from linearity close to $\lambda=0$ and $\lambda=1$.

LD simulations were performed to evaluate the ensemble averages using a time step of 3 fs. As described in Sec. II B, the LD runs are performed using reduced DFT parameters, and then subsequently upsampled using a small number of fully converged calculations. The optimal choice for these reduced DFT parameters was determined by calculating $F^{\rm ah}(V,T)$ for $V=13.87\ {\rm \AA}^3$/atom and $T=3800$ K and finding the smallest values of the reduced DFT parameters which still gave the correct free energy to within ±1 meV/atom upon upsampling. Reduced parameters of 500 eV for the plane-wave cutoff and a grid of $2\times2\times2$ Monkhorst-Pack k points were thus obtained.

Simulations were run until the standard deviation of the canonical ensemble average, $\langle E^{\rm DFT}_{\rm low}-E^{\rm pot}\rangle_\lambda$, was less than 1 meV/atom. The longest runs were necessary for the $T=3800$ K and $\lambda=0$ ensemble averages, with $\approx$1000 LD steps required in these cases. Once calculated for the full set of volume-temperature points, the 25 $F^{\rm ah}(V,T)$ values were used as fitting input for a smooth parametrization of the free energy in terms of a single temperature and volume-dependent Einstein frequency, $\omega^{\rm ah}=a_0+a_1T+a_2V$, with a_0, a_1 and a_2 taken as fitting coefficients [5]. This enables us to take smooth first and second derivatives as required for evaluating the thermophysical properties.

B. Results

From the total energy at $T=0$ K, $E^{\rm tot}$, equilibrium lattice constants of $a=4.658$ Å and $a=4.724$ Å were found within the LDA and GGA, respectively, consistent with previous theoretical results ($a=4.66$ to 4.69 Å for LDA, Refs. [30] and [31], and $a=4.70$ to 4.72 Å for GGA, Refs. [30–34]).

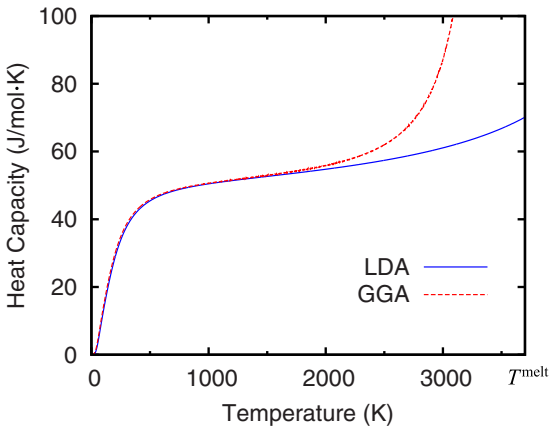

FIG. 1. (Color online) Heat capacity at constant pressure (per mole of formula units) within the quasiharmonic approximation for both LDA and GGA results.

From the quasiharmonic calculations, the thermal properties were found to depend strongly on the choice of exchange correlation functional. This is shown in Fig. 1, where the heat capacity at constant pressure, calculated within the quasiharmonic approximation [i.e., from the free energy $F(V,T)=E^{\rm tot}(V)+F^{\rm qh}(V,T)$], is plotted for both LDA and GGA. One sees a good agreement between the LDA and GGA results up to $T\approx1500$ K; however above this temperature the GGA results increase markedly, diverging at $T\approx3400$ K ($\approx$300 K below the melting point).

The same behavior has been reported previously for Au [35], where the heat capacity calculated within the quasiharmonic approximation diverged in a similar manner for the GGA results. In that work it was found that the inclusion of anharmonic contributions only partially corrected this unphysical divergence, which could be fully removed by including a treatment of exchange and correlation within the random phase approximation (RPA). Application of the RPA, although more costly, is well known to correct some of the shortcomings of the GGA and LDA approximations, but is beyond the scope of the present work. Thus most of the thermodynamic properties have been calculated here only within the LDA, which did not give this spurious divergence with temperature.

Thermal expansion and constant-pressure heat capacity curves are presented in Figs. 2 and 3, respectively, for quasiharmonic (qh), quasiharmonic + electronic (qh+el), and quasiharmonic + electronic + anharmonic (qh+el+ah, or "full vibrational") calculations, alongside the experimental results. The effect of the electronic contribution can be seen by comparing the qh+el and qh curves. For the thermal expansion, the electronic contribution results in only a small change, with the qh+el value at the melting point only 4% larger than the corresponding qh value. For the heat capacity, however, a larger change is found, with the qh+el value at the melting point 15% larger than the qh value.

These results differ from recently published calculations [37], which found a much smaller electronic contribution to the heat capacity ($\approx$1% increase at 3000 K in contrast to an increase of 9% at 3000 K in the present work). This

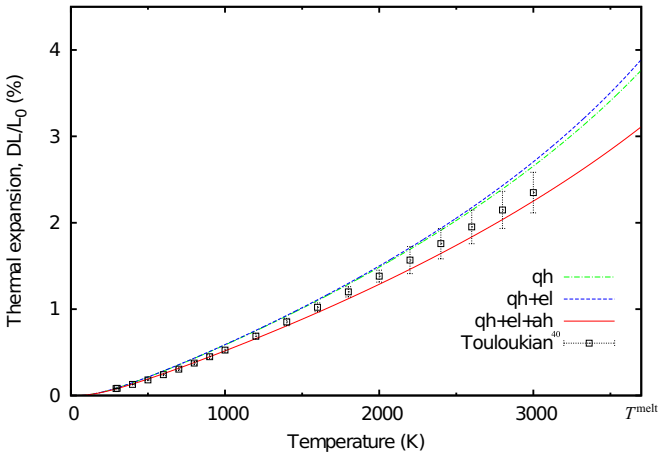

FIG. 2. (Color online) Linear thermal expansion within the LDA for different levels of approximation, including quasiharmonic (qh), quasiharmonic + electronic (qh+el), and quasiharmonic + electronic + anharmonic (qh+el+ah), compared against experimental results.

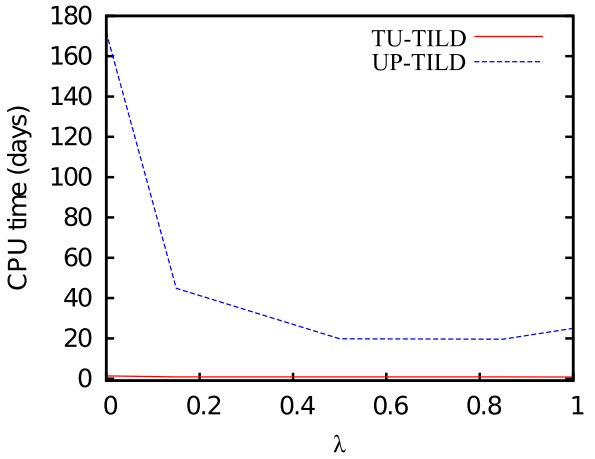

FIG. 4. (Color online) Total time taken to compute $\langle E_{\text{low}}^{\text{DFT}} - E^{\text{pot}} \rangle_{\lambda}$ for $T = 3800$ K and $V = 13.87$ Å^3/atom using 24 cores plotted against the TI coupling parameter, λ. Results are shown for both UP-TILD and TU-TILD methods.

discrepancy was found to be due to the use of different functions to describe the excitation of electrons to states above the Fermi level [36]. We used the Fermi-Dirac distribution here, whereas the original calculations [37] were performed with Methfessel-Paxton smearing [38].

Inclusion of the anharmonic contribution strongly affects both the thermal expansion and heat capacity: The thermal expansion at the melting point is found to be 20% smaller for the full vibrational curve than for the qh+el curve, whereas a reduction of 15% at the melting point is found in the case of the heat capacity. Coincidentally for the heat capacity, the full vibrational results are very close to the quasiharmonic results, with the anharmonic contribution effectively canceling out the electronic contribution, an effect found previously also for other materials [39]. For the thermal expansion this is not the case, with the full vibrational thermal expansion

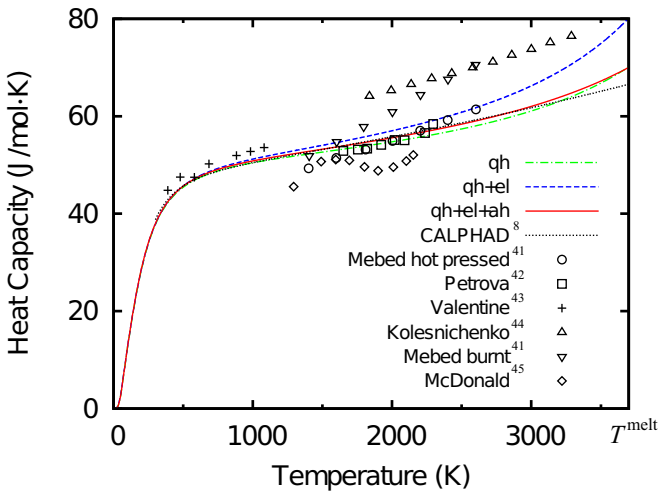

FIG. 3. (Color online) Heat capacity at constant pressure (per mole of formula units) for different levels of approximation, including quasiharmonic (qh), quasiharmonic + electronic (qh+el), and quasiharmonic + electronic + anharmonic (qh+el+ah), compared against experimental results.

significantly lower than both the quasiharmonic and qh+el thermal expansions.

For the thermal expansion the full vibrational results represent an improvement over the qh+el results, with values brought within experimental error of Touloukian's results, which represent a critically assessed average over all of the available experimental data [40]. For the heat capacity, there is a large experimental error associated with the directly measured values [8,41–45], so that in fact both the qh+el and the full vibrational results lie within the scatter of this experimental data. A more useful quantity for comparison in this case is the CALPHAD-derived heat capacity [8]. Within the CALPHAD approach, *all* available experimental data (and associated experimental errors) are incorporated within a single model, which is carefully optimized to provide the best possible fit to the data. Within this approach, the heat capacity is calculated up to the melting point, and the result is found to be in excellent agreement with the full vibrational curve of this work, but in marked disagreement with the qh+el result.

C. Calculation efficiency

The TU-TILD calculations presented here represent a very sizable improvement in efficiency compared to calculations performed within the original UP-TILD scheme. To quantify this improvement, the anharmonic free energy at $T = 3800$ K and $V = 13.87$ Å^3/atom was also computed using the original UP-TILD scheme. The CPU times necessary to compute the corresponding ensemble averages ($\langle E_{\text{low}}^{\text{DFT}} - E^{\text{qh}} \rangle_{\lambda}$ and $\langle E_{\text{low}}^{\text{DFT}} - E^{\text{pot}} \rangle_{\lambda}$ for the original UP-TILD and TU-TILD methods respectively) are then plotted in Fig. 4 as a function of the TI coupling parameter, λ. The TU-TILD approach has reduced computational times to only 24 hours on 24 cores for each λ value, compared to at least 20 days with the original UP-TILD approach. This is also illustrated in Fig. 5, where $\langle E^{\text{pot}} - E^{\text{qh}} \rangle_{\lambda}$ is plotted for $\lambda = 0$ as a function of the number of configurations used to evaluate this average for both MEAM and quasiharmonic references. Taken across all λ, V, and T

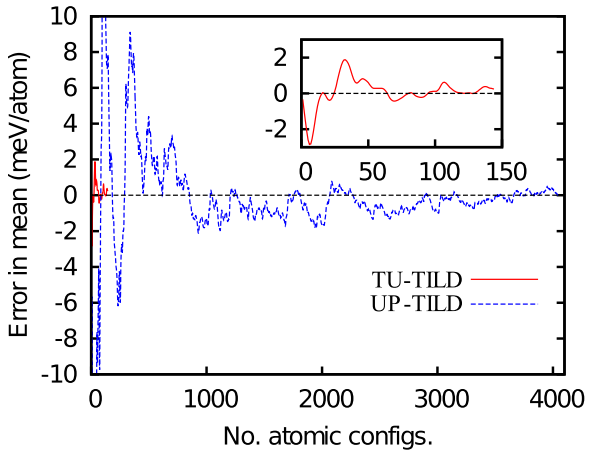

FIG. 5. (Color online) $\langle E^{\rm pot} - E^{\rm qh}\rangle_\lambda$ for $\lambda = 0$, relative to its converged value, plotted against the number of configurations used to evaluate the quantity for both UP-TILD and TU-TILD methods. Inset: Zoomed-in view of the plot at the origin.

values, an overall factor of 50 improvement in efficiency is achieved compared to the original UP-TILD approach.

V. CONCLUSIONS

The thermal expansion and heat capacity of ZrC have been calculated up to its melting point (≈3700 K) using DFT within the local density approximation. The full anharmonicity of lattice vibrations is included, besides the electronic contribution. The effect of anharmonicity is found to be responsible for a reduction in these properties of 20% and 15%, respectively, at the melting point in comparison to quasiharmonic calculations. The anharmonic correction brings the calculated thermal expansion into better agreement with experimental values, and the heat capacity into excellent agreement with CALPHAD results.

The calculations presented here represent an application of the *two-stage upsampled thermodynamic integration using Langevin dynamics* (TU-TILD) approach. In the original UP-TILD approach, a single thermodynamic integration was performed from the quasiharmonic Hamiltonian to the fully anharmonic DFT Hamiltonian. Our approach is to divide the thermodynamic integration into two stages. We use interatomic potentials to describe an intermediate reference state, which is the end point of a first thermodynamic integration from the quasiharmonic reference state and the starting point for a second thermodynamic integration to the fully anharmonic DFT Hamiltonian. This development achieved the same level of accuracy while increasing the efficiency of the calculation by about a factor of 50. The gain in efficiency, although not the value of the final free energy, should depend to some extent on the potential used for the intermediate reference state, for which we adopted a MEAM potential, fitted to the energies of molecular dynamics configurations close to the melting point. The MEAMfit code [22] is freely available for this purpose. Our procedure will be generally applicable to other ultrahigh-temperature ceramics, and indeed to a wide range of materials.

ACKNOWLEDGMENTS

A.I.D., T.D., and M.W.F. would like to thank the EPSRC Program Grant (Grant No. EP/K008749/1) Material Systems for Extreme Environments (XMat) for financial support. D.K., A.G., B.G., and J.N. gratefully acknowledge funding by the European Research Council under the EU's 7th Framework Programme (FP7/2007-2013)/ERC Grant Agreement No. 290998). In addition, M.W.F. acknowledges the support of an Alexander von Humboldt Award. We would like to thank Satoshi Iikubo for helpful correspondence relating to the electronic part of the free energy. This work was funded under the embedded CSE programme of the ARCHER UK National Supercomputing Service (http://www.archer.ac.uk).

[1] H. J. Emeléus, *Advances in Inorganic Chemistry and Radiochemistry* (Academic Press, New York, 1968).
[2] M. W. Barsoum, *The MAX Phases and Their Properties in Ceramics Science and Technology*, Vol. 2 (Wiley-VCH Verlag GmbH & Co., 2010).
[3] P. Souvatzis, O. Eriksson, M. I. Katsnelson, and S. P. Rudin, Phys. Rev. Lett. **100**, 095901 (2008).
[4] A. N. Gandi, Ph.D. thesis, Imperial College London, 2013.
[5] B. Grabowski, L. Ismer, T. Hickel, and J. Neugebauer, Phys. Rev. B **79**, 134106 (2009).
[6] B. Monserrat, N. D. Drummond, and R. J. Needs, Phys. Rev. B **87**, 144302 (2013).
[7] D. Alfè, M. J. Gillan, and G. D. Price, Nature (London) **401**, 462 (1999).
[8] A. F. Guillermet, J. Alloys Compd. **217**, 69 (1995).
[9] B. Grabowski, T. Hickel, and J. Neugebauer, Phys. Rev. B **76**, 024309 (2007).
[10] B. Grabowski, T. Hickel, and J. Neugebauer, Phys. Status Solidi B **248**, 1295 (2011).
[11] B. Grabowski, P. Söderlind, T. Hickel, and J. Neugebauer, Phys. Rev. B **84**, 214107 (2011).
[12] N. D. Mermin, Phys. Rev. **137**, A1441 (1965).
[13] W. Kohn and L. J. Sham, Phys. Rev. **140**, A1133 (1965).
[14] M. I. Baskes, Phys. Rev. Lett. **59**, 2666 (1987).
[15] M. I. Baskes, J. S. Nelson, and A. F. Wright, Phys. Rev. B **40**, 6085 (1989).
[16] B.-J. Lee, M. I. Baskes, H. Kim, and Y. K. Cho, Phys. Rev. B **64**, 184102 (2001).
[17] M. S. Daw and M. I. Baskes, Phys. Rev. Lett. **50**, 1285 (1983).
[18] M. I. Baskes, Phys. Rev. B **46**, 2727 (1992).
[19] M. I. Baskes, Mater. Sci. Eng., A **261**, 165 (1999).

[20] M. Timonova and B. J. Thijsse, Modell. Simul. Mater. Sci. Eng. **19**, 015003 (2011).
[21] The MEAM formalism as presented here deviates slightly from the standard implementation due to the omission of the three-body angular-screening terms.
[22] A. I. Duff, M. W. Finnis, P. Maugis, B. J. Thijsse, and M. H. F. Sluiter, Comp. Phys. Comm. (2015).
[23] G. Kresse and J. Hafner, Phys. Rev. B **47**, 558 (1993).
[24] G. Kresse and J. Hafner, Phys. Rev. B **49**, 14251 (1994).
[25] G. Kresse and J. Furthmüller, Comput. Mater. Sci. **6**, 15 (1996).
[26] G. Kresse and J. Furthmüller, Phys. Rev. B **54**, 11169 (1996).
[27] P. E. Blöchl, Phys. Rev. B **50**, 17953 (1994).
[28] G. Kresse and D. Joubert, Phys. Rev. B **59**, 1758 (1999).
[29] K. Parlinski, Z. Q. Li, and Y. Kawazoe, Phys. Rev. Lett. **78**, 4063 (1997).
[30] K. K. Korir, G. O. Amolo, N. W. Makau, and D. P. Joubert, Diamond Relat. Mater. **20**, 157 (2011).
[31] H. Fu, W. Peng, and T. Gao, Mater. Chem. Phys. **115**, 789 (2009).
[32] N. Rathod, S. K. Gupta, and P. K. Jha, Phase Trans. **85**, 1060 (2012).
[33] Z. Lv, H. Hu, C. Wu, S. Cui, G. Zhang, and W. Feng, Physica B **406**, 2750 (2011).
[34] S. Méçabih, N. Amrane, Z. Nabi, B. Abbar, and H. Aourag, Physica A **285**, 392 (2000).
[35] B. Grabowski, S. Wippermann, A. Glensk, T. Hickel, and J. Neugebauer, Phys. Rev. B **91**, 201103 (2015).
[36] S. Iikubo (private communication).
[37] S. Iikubo, H. Ohtani, and M. Hasebe, Mater. Trans. **51**, 574 (2010).
[38] M. Methfessel and A. T. Paxton, Phys. Rev. B **40**, 3616 (1989).
[39] A. Glensk, B. Grabowski, T. Hickel, and J. Neugebauer, Phys. Rev. Lett. **114**, 195901 (2015).
[40] Y. S. Touloukian and E. H. Buyco, *Thermophysical Properties of Matter*, TPRC Data Series, Vol. 13 (Plenum Press, New York, 1977).
[41] M. M. Mebed, R. P. Yurchak, and L. A. Korolev, Teplofiz. Vys. Temp. **11**, 427 (1973).
[42] I. I. Petrova and V. Y. Chekhovskoi, Teplofiz. Vys. Temp. **16**, 1226 (1978).
[43] R. H. Valentine, T. F. Jambois, and J. L. Margrave, values reported in Ref. [8].
[44] A. P. Kolesnichenko and A. V. Pustogarov, Teplofiz. Vys. Temp. **13**, 1197 (1975).
[45] R. A. McDonald, F. L. Oetting, and H. Prophet, Proc. Meet. Interagency Chemical Rocket Propulsion, Group of Thermochemistry, New York, 1963, CPIA 44, Vol. 1, Johns Hopkins University, Applied Physics Laboratory, Silver Spring, MD, 1954.